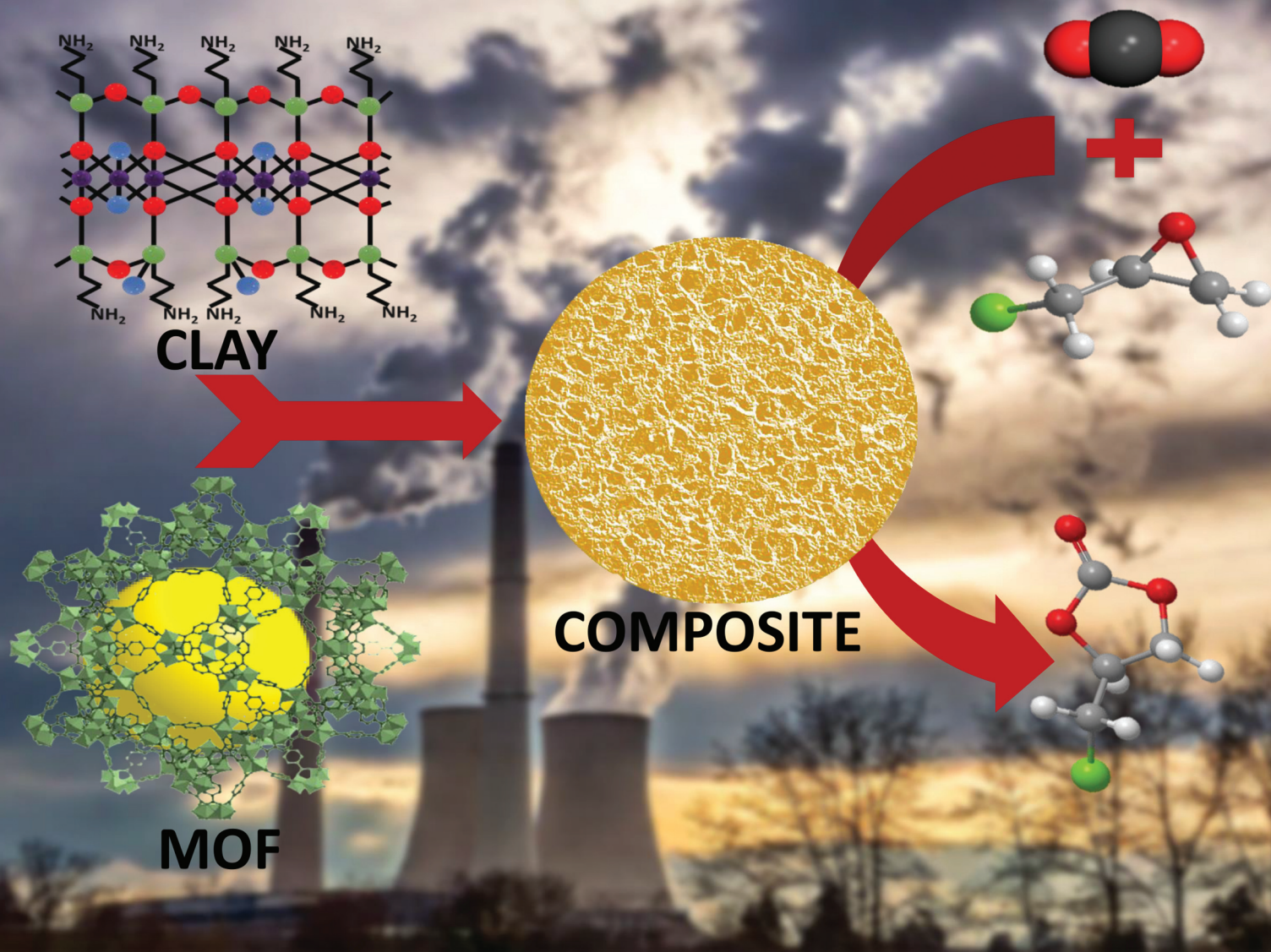


Dalton Transactions




An international journal of inorganic chemistry

rsc.li/dalton



ISSN 1477-9226

PAPER

[View Article Online](#)
[View Journal](#) | [View Issue](#)Cite this: *Dalton Trans.*, 2024, **53**,
15815MIL-101(Cr)/aminoclay nanocomposites for
conversion of CO₂ into cyclic carbonates†Jyoti, ^a Sarita Kumari, ^a Samiran Chakraborty, ^a Prakash Kanoo, ^{a,b}
Vinod Kumar^a and Anindita Chakraborty ^{*,a}

We present the use of an amine functionalized two-dimensional clay *i.e.*, aminoclay (AC), in the chemistry of a three-dimensional metal–organic framework (MOF) *i.e.*, MIL-101(Cr), to prepare MIL-101(Cr)/AC composites, which are exploited as catalysts for efficient conversion of CO₂ gas into cyclic carbonates under ambient reaction conditions. Three different MOF nanocomposites, denoted as **MIL-101(Cr)/AC-1**, **MIL-101(Cr)/AC-2**, and **MIL-101(Cr)/AC-3**, were synthesized by an *in situ* process by adding different amounts of AC to the precursor solutions of the MIL-101(Cr). The composites were characterized by various techniques such as FT-IR, PXRD, FESEM, EDX, TGA, N₂ adsorption, as well as CO₂ and NH₃-TPD measurements. The composites were exploited as heterogeneous catalysts for CO₂ cycloaddition reactions with different epoxides and the catalytic activity was investigated at atmospheric pressure under solvent-free conditions. Among all the materials, **MIL-101(Cr)/AC-2** shows the best catalytic efficiency under the optimized conditions and exhibits enhanced efficacy compared to various MIL-101(Cr)-based MOF catalysts, which typically need either high temperature and pressure or a longer reaction time or a combination of all the parameters. The present protocol using **MIL-101(Cr)/AC-2** as the heterogeneous catalyst gives 99.9% conversion for all the substrates into the products at atmospheric pressure.

Received 22nd March 2024,
Accepted 13th May 2024

DOI: 10.1039/d4dt00849a

rsc.li/dalton

Introduction

CO₂ capture and its subsequent conversion into valuable products offers a unique opportunity to address the serious environmental threats caused by the continuous increase in atmospheric CO₂ level.^{1,2} This approach mitigates the adverse greenhouse effect and creates a circular and sustainable economy by producing important chemicals and fuels.³ In this regard, catalytic CO₂ organic transformation reactions have attracted significant research interest.^{4,5} In particular, the CO₂ cycloaddition reactions with epoxides to produce cyclic carbonates have widely been studied.⁶ The CO₂ cycloaddition reactions typically need a synergy of a Lewis acid catalyst and a Lewis base co-catalyst. Traditional catalysts include metal oxides, metal–porphyrin complexes, lignin-based catalysts and metal–salen complexes.^{6–10} However, most of these catalysts work at elevated temperatures and pressures, and the purifi-

cation and recycling process is also complicated for these homogeneous catalysts.

Over the last few decades, metal–organic frameworks (MOFs) have evolved as novel inorganic–organic hybrid materials with a unique structure and diverse applications.^{11–16} The porous structure, periodicity, highly modular nature and the heterogeneous nature give MOFs an edge over the conventional homogeneous catalysts.^{17–23} The chromium-terephthalate MOF MIL-101(Cr) is a prototype MOF which is well known for its high surface area, hydrothermal and chemical stability and diverse applications.^{24–26} The large mesopores, high thermal stability, good CO₂ adsorption efficacy and the presence of Lewis acidic unsaturated metal sites (UMSSs) available for epoxide binding should make it an ideal catalyst for the cycloaddition reaction of CO₂ with epoxides. However, the crystal field effect makes the Cr(III) centres inert in the octahedral environment, which affects the catalytic efficacy.²⁰ MIL-101(Cr) has been tested as a heterogeneous catalyst for the cycloaddition reactions of CO₂ with epoxides by different research groups and successful reactions mostly require high pressure CO₂ (8–100 bar) in the temperature range 298–393 K, with a reaction completion time of 24–48 h.^{27–30} To use the full potential of the MIL-101(Cr) framework as the desired catalyst, such drastic reaction conditions must be replaced with more ambient conditions, such as room temperature and atmospheric pressure. Recently,

^aDepartment of Chemistry, School of Basic Sciences, Central University of Haryana, Mahendergarh 123031, Haryana, India. E-mail: achakraborty@cuh.ac.in^bSpecial Centre for Nano Sciences, Jawaharlal Nehru University, New Mehrauli Road, New Delhi, Delhi 110067, India†Electronic supplementary information (ESI) available: PXRD, IR spectra, TGA, FESEM images, size histogram plots, the EDX spectrum, pore size distribution, CO₂-TPD and NH₃-TPD, ¹H NMR spectra, tables and reaction schemes. See DOI: <https://doi.org/10.1039/d4dt00849a>

MIL-101 composites with polyoxometalates, ionic liquids and ionic polymers have shown enhanced catalytic properties;^{31–47} however, with the synergy of an easy synthetic method, efficient catalytic conversion at ambient temperature and atmospheric pressure in a quick time is yet to be achieved. We aimed to obtain enhanced catalytic CO₂ conversions under ambient conditions using new composites based on the robust and porous structure of MIL-101(Cr). Novel MOF composites mitigate the typical shortcoming of MOFs like moisture sensitivity, poor water dispersibility, and poor thermal and chemical stability and exhibit enhanced/new properties based on judicious blending of MOFs with other functional components.^{48,49} We envisage that a synergistic combination of 2D layered clay, aminoclay (AC)⁵⁰ with MIL-101(Cr) could result in such composites. Aminopropyl functionalized magnesium phyllosilicate (Scheme 1), popularly known as aminoclay (AC), has recently shown its potential to form novel MOF nanocomposites having enhanced CO₂ adsorption, separation and catalytic conversion properties.^{51–53} In the present work, we report the synthesis of new MIL-101(Cr)/AC nanocomposites and their efficacy for CO₂-epoxide cycloaddition reactions (Scheme 1). Three different composites were synthesized under solvothermal conditions by adding different amounts of AC to the precursor solution, MIL-101(Cr). The composite **MIL-101(Cr)/AC-2** exhibits the best performance showing 99.9% conversion in the cycloaddition reaction of epichlorohydrin (EPH) with CO₂ in 6 h at atmospheric pressure and 30 °C, while the pristine MOF shows a conversion of only 30% under the same reaction conditions. **MIL-101(Cr)/AC-2** has also been tested as a heterogeneous catalyst using several other epoxide substrates and 99.9% conversion could be

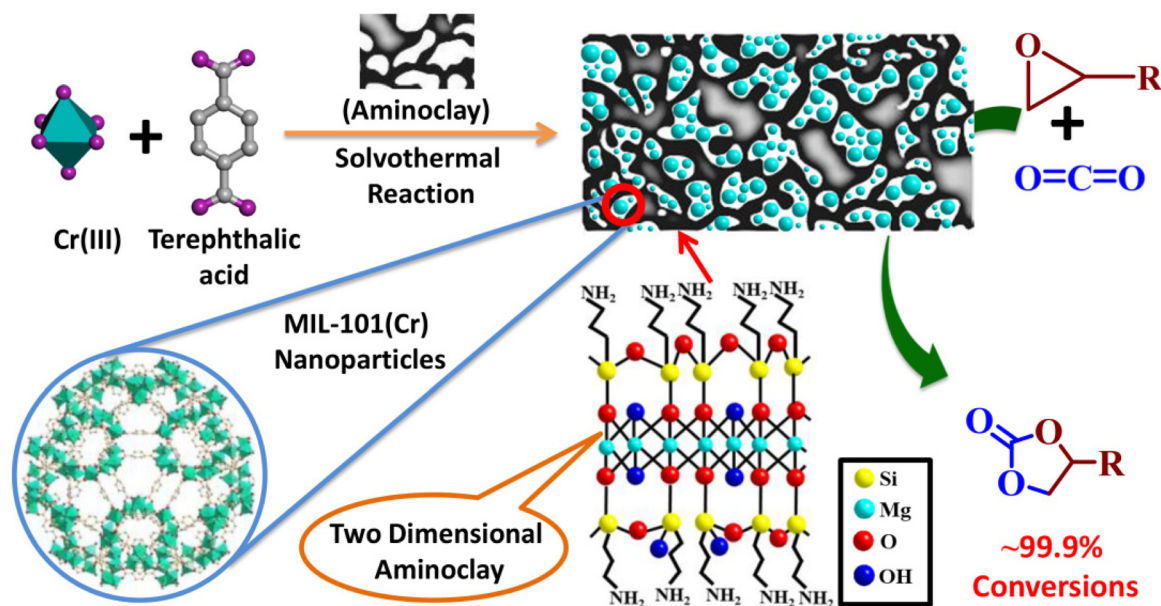
achieved with all the substrates under ambient reaction conditions.

Results and discussion

Synthesis and phase-purity of the composites

Pristine MIL-101(Cr) (**PMIL**) and aminoclay (AC) were synthesized by following the literature reported procedures.^{54,55} To synthesize the composites, a simple and facile *in situ* procedure was adopted where AC was dispersed in water first followed by the addition of the precursors of **PMIL**, which were then reacted under solvothermal conditions (see the Synthesis section for details). Three different composites named **MIL-101(Cr)/AC-1**, **MIL-101(Cr)/AC-2** and **MIL-101(Cr)/AC-3** were synthesized by successively increasing the relative amount of AC in the reaction mixtures. The well-correspondence between the simulated and experimental PXRD patterns (Fig. 1) of **PMIL** suggests high purity of the obtained sample. All the three composites exhibit PXRD patterns similar to that of **PMIL** (Fig. 1), indicating the formation of a pure phase of **PMIL** in the composites.

The presence of the AC in the composites is difficult to interpret from the PXRD patterns as AC is weakly diffracting compared to the highly crystalline MOF and also the minor phase in the composites. However, with the increase in AC content, we observed the appearance of a broad reflection at $2\theta = 37^\circ$ in the composites with a higher clay content (particularly in **MIL-101(Cr)/AC-3**), which is attributed to the presence of the AC phase in the composite. This $2\theta = 37^\circ$ reflection is also observed in the PXRD pattern of the AC (Fig. S1†), which



Scheme 1 Synthesis of the self-assembled MIL-101(Cr)/AC composites, where the nanoparticles (NPs) of MIL-101(Cr) are assembled through the aminoclay (AC) layers. The composites are exploited as catalysts for the CO₂ cycloaddition reaction with epoxides to produce cyclic carbonates. The structures of MIL-101(Cr) and AC are also shown in the scheme.

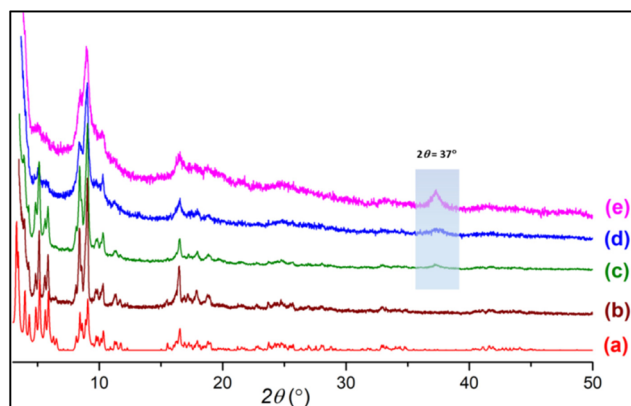


Fig. 1 PXRD patterns of (a) simulated **PMIL**, (b) as-synthesized **PMIL**, (c) **MIL-101(Cr)/AC-1**, (d) **MIL-101(Cr)/AC-2** and (e) **MIL-101(Cr)/AC-3**.

is ascribed to the $d_{130,200} = 0.238$ nm reflection originating from the 2 : 1 trioctahedral Mg-phylosilicate clay with a talc-like structure of AC.⁵⁰

IR spectra and thermal stabilities of the composites

To ascertain the functional groups of the samples, FT-IR spectra were recorded (Fig. 2 and S2†). The spectrum of **PMIL** shows the characteristic peaks of MIL-101(Cr) as reported in the literature.^{48,56} The IR spectrum of AC suggests its characteristic organoclay structure (Si–C 1116 cm^{-1} , Si–O–Si 1014 cm^{-1})^{50,51} with the presence of a broad N–H stretching frequency band ($\sim 3200\text{--}3700$ cm^{-1}) (Fig. S2†). The IR spectra for all the composites are very similar to that of the **PMIL**, with intense bands appearing in the range of $\sim 1400\text{--}1625$ cm^{-1} , which are corresponding to the stretching frequency of the carboxylate group of the 1,4-benzenedicarboxylate (H_2bdc) ligand, originating from the **PMIL**. Selected FT-IR peaks (in cm^{-1}) of **MIL-101(Cr)AC-1**: 1625 s, 1509 m, 1398 s, 1090 w, 1050 m, 1016 m, 883 m, 831 w, 745 s (Fig. S2†). Distinct bands around 1090 cm^{-1} and 1050 cm^{-1} appeared for the composite (which are absent in **PMIL**) and are ascribed to the Si–C and Si–O–Si

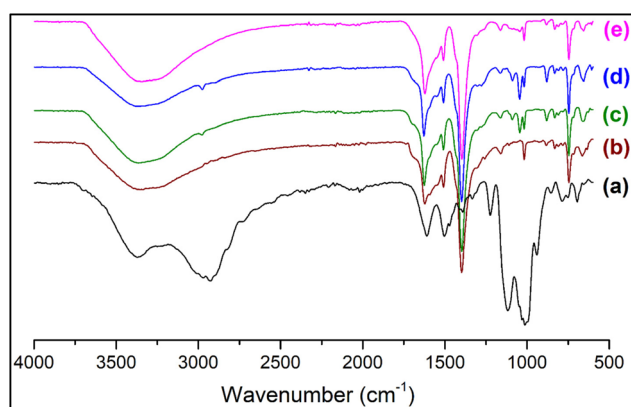


Fig. 2 FTIR spectra of (a) aminoclay, (b) as-synthesized **PMIL**, (c) **MIL-101(Cr)/AC-1**, (d) **MIL-101(Cr)/AC-2** and (e) **MIL-101(Cr)/AC-3**.

stretching, respectively, and these bands originate from the AC phase (Fig. S2†). The shift in the above two vibrations in the composite compared to that in the pristine AC may be attributed to the plausible interaction of the NH_2 groups of AC with the Cr(III) centres of the MOF. We envisage that in the composite, the nitrogen atoms of NH_2 groups interact with Cr(III) centres and pull the alkyl chain towards itself leading to the weakening of the Si–C bond, which is reflected in the lower wavenumber (1090 cm^{-1}) in the composite, compared to that of AC (1014 cm^{-1}). On the other hand, the drift of the electron density of the alkyl chain towards Cr(III) makes Si atoms relatively electronegative which consequently pulls the oxygen atoms towards itself making the Si–O bond stronger, shifting it to a higher wavenumber (1050 cm^{-1} in the composite vs. 1014 cm^{-1} in AC). The IR spectra of other composites are similar to that of **MIL-101(Cr)AC-1** and suggest the presence of both **PMIL** and the AC phase.

To investigate the thermal stabilities of the samples, thermogravimetric analyses (TGA) (Fig. S3†) of the as-synthesized **PMIL** sample and all the composites were carried out. **PMIL** exhibits an initial weight loss of about 41% up to 100 $^{\circ}\text{C}$, which matches well with the literature value and corresponds to a loss of ~ 25 solvent (H_2O) molecules from the framework.^{32,54} The dehydrated framework shows a plateau up to 350 $^{\circ}\text{C}$ temperature, beyond which framework decomposition occurs. All the composites exhibit similar profiles for thermal stability to that of **PMIL** and are stable up to the temperature range of 350–360 $^{\circ}\text{C}$, which suggests that the composite formation does not affect the thermal stability of the framework structure. However, the initial weight loss percentages (Fig. S3†) for the composites are different compared to that of **PMIL**. The lesser initial loss may be attributed to the presence of a relatively small amount of the highly porous and solvated **PMIL** phase in the composites, where the AC content increases from **MIL-101(Cr)/AC-1** to **MIL-101(Cr)/AC-3**, which is consistent with the synthetic conditions where an increasing amount of AC was added in the reaction mixtures for the latter composites.

Textural properties of the composites

The as-synthesized **PMIL** particles are known to be octahedral and nanometer-sized, as reported in the literature.³² We recorded the FESEM images for our as-synthesized **PMIL**, which reveal that faceted octahedral-like particles are present having sizes in the range of 100–150 nm (Fig. S4†). A literature survey suggests that the FESEM images of AC exhibit a typical layered structure attributed to the 2D sheet-like organoclay structure.⁵⁰ To get an idea about the morphology of the composites, FESEM images were recorded for all the composites, which show a distinct difference compared to both **PMIL** and AC. For **MIL-101(Cr)/AC-1**, an assembly of fused particles is observed, where the MOF nanoparticles (NPs) appeared to be coated with AC layers (Fig. 3a, b and S5†). Such a morphology is in clear contrast to the faceted particles of the pristine framework. The size histogram plot (Fig. S6†) shows that the particles have a maximum distribution in the size range of

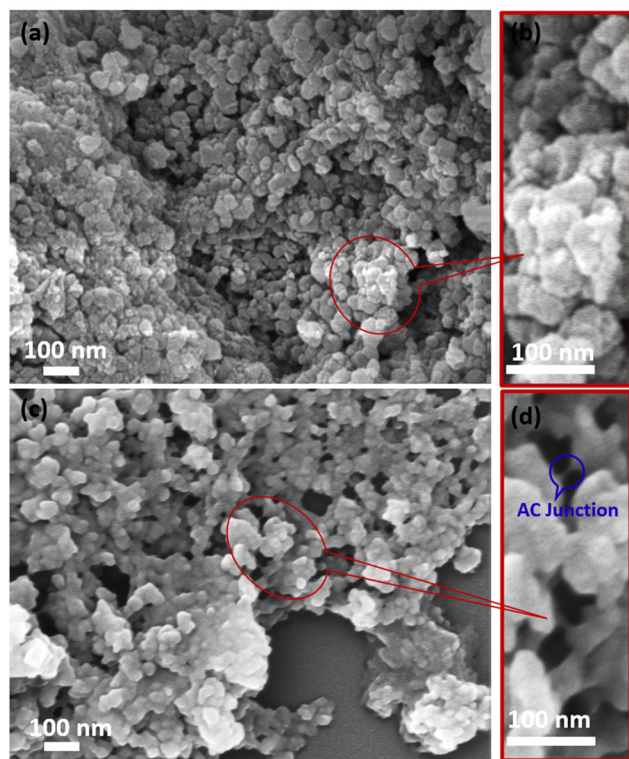


Fig. 3 (a) FESEM images of composite MIL-101(Cr)/AC-1, (b) magnified view of a portion from MIL-101(Cr)/AC-1 showing the AC coated fused particles, (c) FESEM images of composite MIL-101(Cr)/AC-2 and (d) magnified view of a portion from MIL-101(Cr)/AC-2 showing the presence of layered AC junctions between the PMIL NPs.

70–90 nm. The assembly of particles is more evident in the case of MIL-101(Cr)/AC-2, where distinct faces of the PMIL particles disappear and the particles gradually become more spherical-like particles, with an increase in the AC content in the composite (Fig. 3c, d and S7†). The AC layer coating PMIL is visible in the case of MIL-101(Cr)/AC-2 in the presence of layered AC junctions between the PMIL NPs (Fig. 3d). We envisage that the assembly of the PMIL particles through AC in the composites occurs due to the specific interaction between unsaturated surface functionalities (e.g., Cr³⁺ sites) in the PMIL NPs and the amine-functionalized clay, which results in a self-assembled MOF–clay nanocomposite. To the best of our knowledge, only one report is known so far to document such self-assembled nanocomposites, where the MOF (ZIF-8) particles were ‘glued’ by clay (AC) driven by the interaction between the Zn²⁺ sites of ZIF-8 and the NH₂ groups of AC.⁵¹ The size histogram plot reveals that the maximum particles of MIL-101(Cr)/AC-2 have sizes in the range of 50–70 nm (Fig. S8†). It is noteworthy that the average sizes of particles decrease in the order: PMIL < MIL-101(Cr)/AC-1 < MIL-101(Cr)/AC-2. This may be attributed to the downsizing efficacy of AC through coordination modulation *via* the NH₂ group, as literature reports indicate that AC can also act as a functional template to assist growth of MOF NPs.⁵² The FESEM images of MIL-101(Cr)/AC-3 exhibit that NPs are also fused similar to the

first two composites, but with an increased amount of AC coating (Fig. S9†). This is attributed to the use of excessive AC in the reaction mixture, which results in an inhomogeneous composite having too much AC content. It's difficult to comment on the size of the particles in MIL-101(Cr)/AC-3, as the PMIL particles are highly coated and deeply buried in the increased number of AC layers.

To understand the element content and their distribution, we performed an energy dispersive X-ray (EDX) study and element analysis for one of the composites, MIL-101(Cr)/AC-2. The EDX spectrum (Fig. S10†) clearly shows the presence of Mg and Si elements coming from AC and Cr from PMIL and thus confirms the presence of both the parent materials (PMIL and AC) in the composite. Furthermore, elemental mapping indicates that the different elements are distributed uniformly throughout the sample, suggesting the formation of a homogeneous composite (Fig. 4). The homogeneous nature of MIL-101(Cr)/AC-2 prompted us to check its solution processability, as enhanced dispersibility can be expected from such a homogeneous composite. When the same amount of PMIL and MIL-101(Cr)/AC-2 was dispersed in methanol (5 mg in 2 ml), PMIL settled down within 15 min, but the dispersion of MIL-101(Cr)/AC-2 remained stable even after 4 days (Fig. S11†). This result clearly demonstrates the high solution processability of the composite.

Adsorption and TPD studies

In order to investigate the porous nature and to know the surface area of the samples, N₂ adsorption isotherms at 77 K of the activated PMIL and the composites were recorded (Fig. 5). The as-synthesized PMIL sample shows high uptake of N₂ gas and a typical type-1 profile with a BET surface area of 2300 m² g^{−1}. The value of the surface area is consistent with the literature reported values^{5,25} of MIL-101(Cr). On the other hand, the densely packed 2D layers of AC are known to inhibit any N₂ uptake at 77 K (ref. 51–53) and exhibit negligible N₂ uptake (Fig. 5). MIL-101(Cr)/AC-1 exhibits a type-I profile, but the total uptake (~800 cc g^{−1}) at P/P₀ = 1 and the BET surface area (1434 m² g^{−1}) are much lower than those of PMIL. Such a decrease in the surface area is attributed to the presence of the non-porous AC phase in the composite. Similarly, the other two composites also exhibit type-I profiles with lower N₂ uptake (Fig. 5), and the uptake gradually decreases with an increase in AC content from MIL-101(Cr)/AC-1 to MIL-101(Cr)/AC-3. The BET surface areas are found to be 1332 m² g^{−1} and 921 m² g^{−1} for MIL-101(Cr)/AC-2 and MIL-101(Cr)/AC-3, respectively. Furthermore, the pore size distribution plot (Fig. S12†) of the PMIL and all the MIL-101(Cr)/AC composites shows the presence of characteristics pores of the MIL-101(Cr) framework (~29 Å and ~34 Å) which matches well with the literature.²⁴ In the case of MIL-101(Cr)/AC-2, we observed a broad distribution centered near ~45 Å and we attribute this to the formation of some random large pores at the MOF–clay interface, which may also enhance the substrate diffusion and enhance the catalytic efficacy.

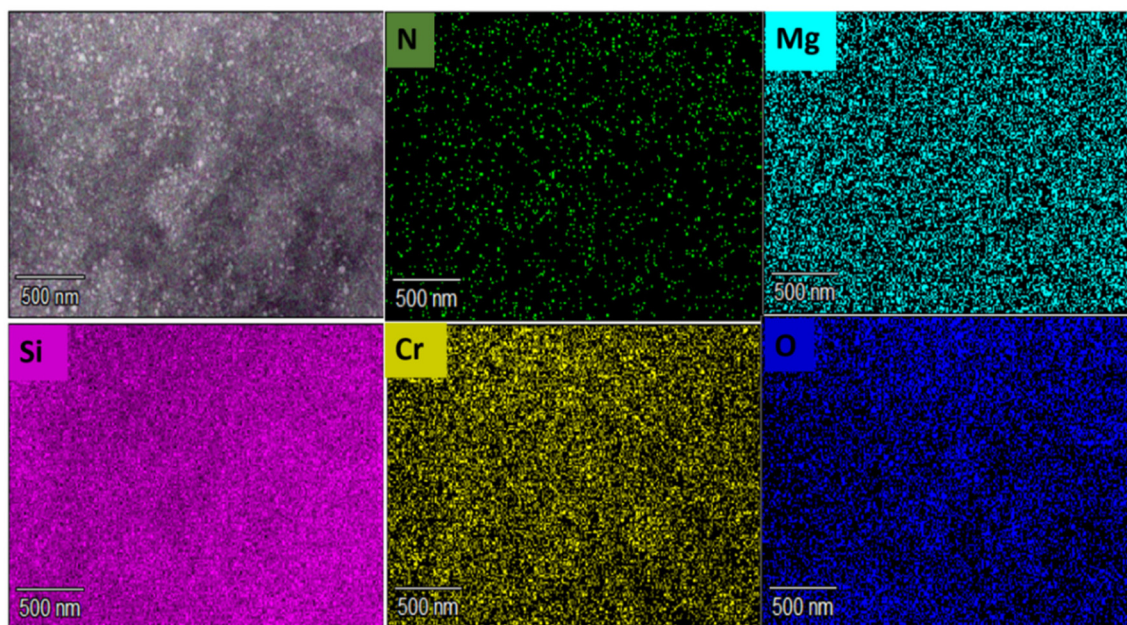


Fig. 4 Elemental mapping of MIL-101(Cr)/AC-2 indicating uniform distribution of various elements (Cr, Mg, Si, N, O) throughout the material.

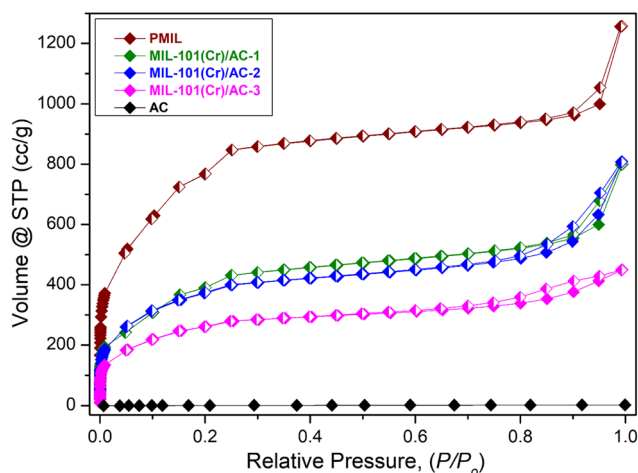


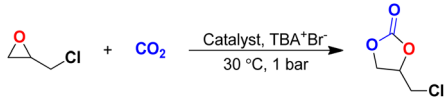
Fig. 5 N_2 Adsorption isotherms of PMIL, MIL-101(Cr)/AC-1, MIL-101(Cr)/AC-2, MIL-101(Cr)/AC-3 and AC at 77 K. Open symbol denotes adsorption and closed symbol denotes desorption of gas molecules.

To investigate the presence of any Lewis acidic and basic sites in MIL-101(Cr)/AC-2, we performed TPD experiments with NH_3 and CO_2 (Fig. S13[†]). The acidity and basicity were determined from the peak area of the desorbed NH_3 and CO_2 . The NH_3 -TPD profile shows a desorption peak in the temperature range of 30–350 °C with 1.629 mmol g^{-1} of desorption capacity, suggesting moderate acidic sites, which may be attributed to the Cr(III) UMSs. The CO_2 -TPD profile shows a desorption peak in the temperature range of 200–350 °C with 1.125 mmol g^{-1} of desorption capacity, suggesting the presence of moderate basic sites in the composites, which may be attributed to the NH_2 groups at the MOF-clay interface.

Catalytic study

We envisage that the composites, particularly MIL-101(Cr)/AC-2, can be efficient as a catalyst for the CO_2 conversion, as the catalytic reaction can occur at pores as well as at the surface of the composite and at the MOF-clay interface where the basic NH_2 groups are present. The synergy of Lewis acidic Cr(III) UMS and Lewis basic NH_2 sites was expected to enhance the catalytic activity.

For a comparative study, we studied the catalytic performance of all the composites, along with the pristine MOF (PMIL) and AC in the CO_2 cycloaddition reactions with epoxides, using tetrabutylammonium bromide (TBA^+Br^-) as a co-catalyst under solvent-free conditions and conversion (%) for the product formation was calculated using the 1H NMR spectrum (see the Experimental section for details). To start with, EPH as the model epoxide substrate (Table 1) was selected and catalytic reactions were performed with different catalysts under the identical optimized reaction conditions. AC shows only 10% catalytic activity (entry 1, Table 1), while a Cr(III) salt exhibits only 27% conversion (entry 2, Table 1) up to 6 h, and the catalyst is homogeneous. The heterogeneous catalyst PMIL exhibits only a slight increase in the conversion (entry 3, Table 1) compared to that of the homogeneous Cr(III) salt, and the poor conversion (30%) can be attributed to the inertness of the Cr(III) centres of PMIL, which typically needs high CO_2 pressure for the cycloaddition reaction.^{32,35,51} To our delight, under the same reaction conditions, the composites exhibit an enhanced performance compared to the PMIL. MIL-101(Cr)/AC-1, MIL-101(Cr)/AC-2 and MIL-101(Cr)/AC-3 show conversions of 44, 99.9 and 42%, respectively (entries 4–6, Table 1) in 6 h and the conversion (%) was calculated using 1H NMR spectra (Fig. S14[†]). We also recorded the FT-IR spectra (Fig. S15[†]) of the model substrate *i.e.*, EPH and the reaction mixture of the product in the cycloaddition reaction of

Table 1 Results of cycloaddition of CO₂ with EPH using the as-synthesized PMIL and MIL-101(Cr)/AC composites as catalysts^a


Entry	Catalysts	Time (h)	Conversion (%)
1	Aminoclay	6	10
2	Cr(NO ₃) ₃ ·9H ₂ O	6	27
3	PMIL	6	30
4	MIL-101(Cr)/AC-1	6	44
5	MIL-101(Cr)/AC-2	6	99.9
6	MIL-101(Cr)/AC-3	6	42
7	PMIL + AC ^b	6	5
8	TBAB ^c	6	20
9	TBAB ^d	6	30

^a Reaction conditions: 9.2 mmol (851 mg) EPH, 30 mg activated catalyst and 0.92 mmol (296 mg) TBA⁺Br[−] under 1 bar CO₂ and 30 °C.

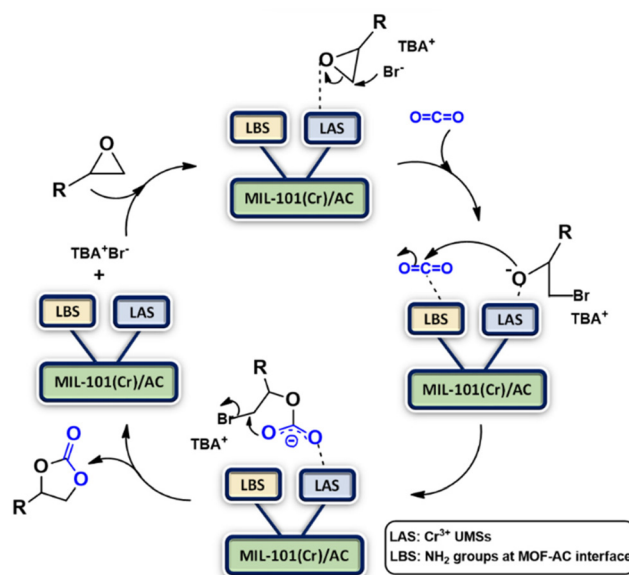
^b Physical mixture. ^c Without the catalyst at 30 °C. ^d Without the catalyst at 40 °C. Conversion (%) were calculated from the ¹H NMR spectra by integration of epoxide peaks *versus* cyclic carbonate peaks.

EPH with CO₂ using the **MIL-101(Cr)/AC-2** catalyst. The IR spectra (Fig. S15†) clearly suggest the conversion of the EPH to the cyclic carbonate product exhibiting the characteristic carbonyl stretching frequency at 1783 cm^{−1} arising from the carbonate group of the product. To confirm that the enhanced catalytic efficacy is indeed the effect of the composite formation, an experiment under the same reaction conditions was carried out, using a physical mixture of **PMIL** and AC as the catalyst (entry 7, Table 1). This physical mixture exhibits a negligible conversion (5%) of the substrate. This observation clearly indicates that a physical mixture does not have the synergistic effect as in the case of a composite. Such negligible conversion may be attributed to the densely packed non-porous AC layers in the mixture which inhibit accessibility to the catalytic sites. The catalytic reaction without any catalyst and only using the co-catalyst, TBA⁺Br[−], was also performed at 30 °C and 40 °C (entries 8 and 9, Table 1), which shows only 20% and 30% conversion within 6 h, respectively. Reactions were also performed using the catalyst (**MIL-101(Cr)/AC-2**) only at 30 °C and we got negligible conversion (entry 29, Table S1†), suggesting that the presence of the co-catalyst is essential for effective reaction. Apart from TBAB as a co-catalyst, we also tried catalytic reactions using other co-catalysts such as tetrabutylammonium chloride (TBAC) and tetrabutylammonium iodide (TBAI) to compare the effectiveness of the co-catalyst on the catalytic activity of the reaction. An ideal co-catalyst for catalytic reaction should have suitable nucleophilicity as well as better leaving group ability. Upon co-catalyzing the CO₂/EPH cycloaddition with TBAC, we observed a conversion of approximately 50% within 6 h and 80% within 24 h. However, when employing TBAI, the conversion was only around 5% within 6 h, with a subsequent increase to 50% after 24 h of reaction, while the reaction is completing within 6 h using TBAB as a co-catalyst. From our observations the enhanced efficiency of TBAB over TBAI may be attributed to its smaller molecular size, which

enables facile diffusion within the confined channels of the MOF structure. Additionally, the observed superiority of TBAB compared to TBAC could be attributed to the better leaving group ability of bromide ions in TBAB, which facilitates the ring-opening reaction and subsequent carbonate formation more effectively. The efficient catalytic activity of TBAB as a co-catalyst may be attributed to the less energy barrier for opening of the epoxide ring of the substrate for the addition of CO₂. So, the intricate interaction among molecular properties emphasizes the impact of co-catalysts on determining the effectiveness of the cycloaddition reaction.^{57–60} We have also conducted an additional experiment to evaluate the catalytic performance of **MIL-101(Cr)/AC-2** with EPH at an elevated temperature (at 70 °C). As a result of our analysis, we observed that the CO₂ cycloaddition reaction is accomplished in 5 h at 70 °C. This indicates that the temperature has minimal impact on the catalytic reaction under the optimized conditions, as it also reaches completion within 6 h at 30 °C.

Among all the composites, **MIL-101(Cr)/AC-2** shows the best performance owing to its homogeneous structure having a uniform distribution of the different elements, as revealed by the FESEM images. Furthermore, this composite also exhibits the smallest size particles (50–70 nm) among all the composites, and the network structure of the fused small NPs is expected to enhance the substrate diffusion to the catalytic sites, as the catalytic efficacy is found to be high for well-dispersed MOF NPs.^{51,61,62} Finally, the synergy of the Lewis acidic Cr(III) UMSs and the Lewis basic NH₂ groups, as revealed by the TPD experiments, is expected to enhance the catalytic efficacy in this composite.

A plausible mechanism for CO₂-epoxide cycloaddition using the MIL-101(Cr)/AC composites as catalysts is presented in Scheme 2. This involves coordination of an epoxide oxygen atom with a Lewis acidic site (LAS), which is the Cr(III) UMS in

**Scheme 2** Proposed mechanism for cycloaddition of CO₂ with epoxides catalyzed by **MIL-101(Cr)/AC-2** involving LASs, LBSs and TBA⁺Br[−].

the composite structure. This results in polarization of the C–O bond and subsequently Br^- of the co-catalyst (TBA^+Br^-) attacks the less sterically hindered carbon atom of the epoxide nucleophilically, causing a heterolytic cleavage. Subsequently, the CO_2 carbon atom is activated by the Lewis basic site (LBS), which we assign to the NH_2 groups in the composite structure, which are possibly present at the MOF–clay interface. This facilitates the nucleophilic attack on the CO_2 carbon atom by the ring-opened alkoxide intermediate. This process allows carbon dioxide to enter and intramolecular ring-closure takes place to produce cyclic carbonate, regenerating the catalyst and co-catalyst.

The conversion decreases from **MIL-101(Cr)/AC-2** to **MIL-101(Cr)/AC-3**, which is attributed to the inhomogeneous nature of **MIL-101(Cr)/AC-3**, however it still shows a considerable conversion (comparable to that of **MIL-101(Cr)/AC-1**). To study the reaction completion time using each of the composites as a catalyst, we continued the reactions for a longer time and the conversions were recorded at regular time intervals (entries 15 and 25, Table S1, Fig. S16 and S17†). We also checked the heterogeneity of one of the composites, **MIL-101(Cr)/AC-2**. To confirm the heterogeneity for the catalytic process of the cycloaddition reaction of EPH, filtration tests were carried out. After 1 h of catalytic reaction at 1 bar of CO_2 and at temperature 30 °C, the solid catalyst was removed, and a conversion of 33% was obtained. The catalytic reaction was further continued with the filtrate and it was observed that after removal of the solid catalyst, the conversions were 36, 37, 38, 39 and 40% at 2, 3, 4, 5 and 6 h, respectively, which clearly indicates that there is no significant conversion after the filtration (Fig. 6). On the other hand, the undisturbed catalyst shows conversions of 43, 63, 69, 92 and 99.9% at 2, 3, 4, 5 and 6 h, respectively (Fig. 6). These observations further confirm the heterogeneity of the catalyst. The recyclability test was also performed with the recycled **MIL-101(Cr)/AC-2** catalyst in the cycloaddition reaction of EPH with CO_2 and no significant

decrease in the catalytic conversion was observed up to five cycles (88% conversion after the 5th cycle) (Fig. 7). Following each catalytic run, the heterogeneous catalyst can be effectively recovered from the reaction mixture by filtration and can be reused without losing its active properties. When comparing with the recovered catalyst's PXRD and FTIR data (Fig. S18 and S19†) with that of the **MIL-101(Cr)/AC-2**, no significant changes were observed, implying that the catalyst's structural integrity has not been compromised.

The superior catalytic performance of **MIL-101(Cr)/AC-2** inspired us to further expand the application of this novel composite as a catalyst in the cycloaddition of CO_2 with other epoxides. After the catalytic reaction with EPH, we carried out a catalytic reaction with styrene oxide (SO) which is a larger rigid epoxide with a bulky phenyl ring attached to it. Under the optimized reaction conditions for EPH, there was no significant conversion with both the **PMIL** and the composite while SO was used as the substrate. Therefore, we carried out this reaction at a little elevated temperature (*i.e.*, 40 °C) which resulted in good CO_2 conversion efficiency for **MIL-101(Cr)/AC-2**. CO_2 conversion using **PMIL** was also carried out at 40 °C with SO keeping all other conditions the same. In the first few hours (*i.e.*, up to 12 h), **PMIL** does not show any conversion, but the composite shows significant conversion (60% at 12 h). As the reaction continued, **PMIL** shows a little conversion (5, 12, and 15% at 24, 42 and 48 h, respectively), whereas **MIL-101(Cr)/AC-2** shows conversion of 71.4, 92.5 and 99.9% at 24, 42 and 48 h, respectively (Fig. 8 and Table S2†).

These results also indicate that the catalytic activity is significantly enhanced for the composite when a bulkier substrate is taken. The optimization of reaction conditions with various other substrates was also performed and we observed that, some of the substrates were not showing efficient catalytic activity at 30 °C and required a little elevated temperature (40 °C), which may be attributed to the different sizes

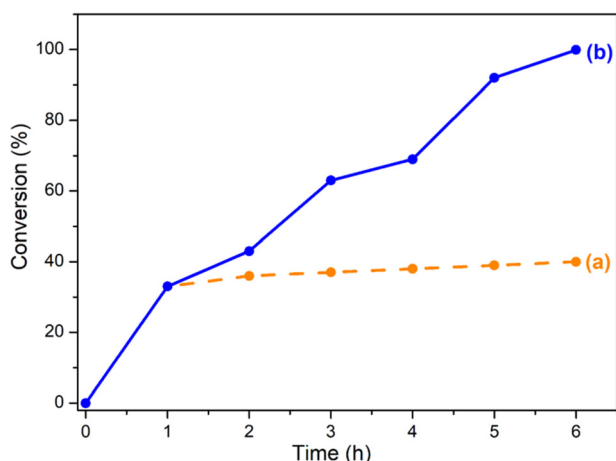


Fig. 6 CO_2 conversion % with EPH (a) catalyst **MIL-101(Cr)/AC-2** removed after 1 h of catalytic reaction and (b) reaction continued undisturbed with catalyst **MIL-101(Cr)/AC-2** up to 6 h.

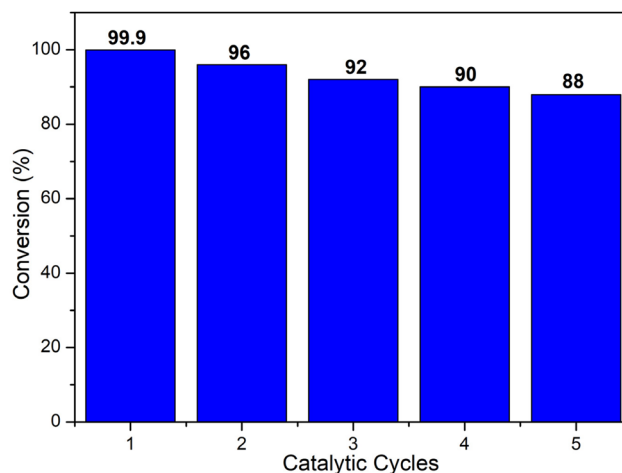


Fig. 7 Recyclability test using **MIL-101(Cr)/AC-2** as a catalyst for the cycloaddition reaction of CO_2 with EPH. Identical reaction conditions to those of Table 1 were employed.

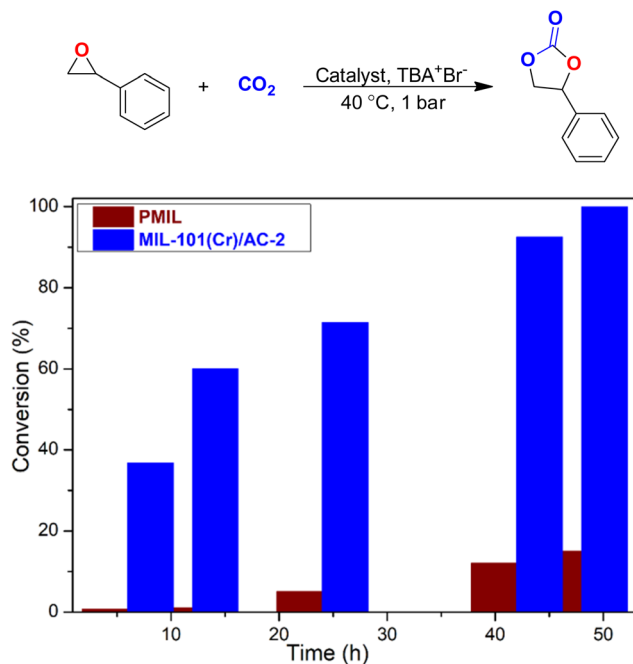


Fig. 8 Conversion as a function of time using **PMIL** and **MIL-101(Cr)/AC-2** as catalysts for the cycloaddition reaction of CO₂ with SO. Conversion (%) were calculated from the ¹H NMR spectra by integration of epoxide versus cyclic carbonate peaks.

(Table S3†) and reactivities of the substrates. The catalytic activity of the **MIL-101(Cr)/AC-2** catalyst was examined (Table 2). It was observed that the small epoxides [propylene oxide (PO) and epoxy butane (EB)] undergo full conversion (99.9%) within 6 h (entries 2 and 3, Table 2), whereas for larger or bulkier epoxides [allyl glycidyl ether (AGE), butyl glycidyl ether (BGE)] (Table S3†), the reactions are relatively slow, but also shows full CO₂ conversion when the reaction time is extended up to 12 h for AGE and 15 h for BGE at 40 °C (entries 4 and 5, Table 2).

In general, the percentage conversion decreases as the size of the substrate molecule (Table S3†) increases. It becomes difficult for bigger molecules to interact with Cr(III) because of the steric hindrance and can be considered as a key factor of barrier for the interaction of the epoxide with the chromium center in the catalyst.⁶³ The results indicate that efficient conversion of the bulky substrates can be achieved using elevated temperatures and an extended reaction time.

From the above results, the features of **MIL-101(Cr)/AC-2** as a heterogeneous catalyst for the CO₂ conversion reaction can be summarized as below:

- Excellent conversion at ambient temperature and atmospheric pressure while the parent MOF catalyst typically requires high temperature and pressure.
- Complete conversion in a shorter reaction time.
- Enhanced solution dispersibility and processability (compared to the parent MOF).
- Easy recyclability as compared to other traditional organic homogeneous catalysts.

The above advantages make our composite indeed a better catalyst than the pristine MOF. In order to compare the efficiency of **MIL-101(Cr)/AC-2** as a catalyst towards the CO₂ conversion reactions with respect to the reported MIL-101(Cr) and MIL-101(Cr)-based MOF catalysts, a literature survey was done and the results are summarized in Table S4.† Table S4† indicates that most of the pristine MOF catalysts need relatively higher temperatures (30–100 °C) and high pressure (5–20 bar) for the CO₂-epoxide cycloaddition reactions. The catalyst **MIL-101(Cr)/AC-2** presents almost complete conversion comparatively in less time and under ambient reaction conditions. Thus, our composite catalyst would be the one of the best candidates among the MIL-101(Cr) based materials.

Conclusions

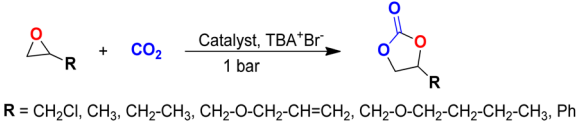
In summary, this work showcases the synthesis of new MIL-101(Cr)-Aminoclay composites and their utilization as heterogeneous catalysts for efficient conversion of CO₂ gas into valuable cyclic carbonates. The highly porous and robust framework of MIL-101 is a well-studied prototype MOF containing Lewis acidic Cr(III) sites, but when employed as a heterogeneous catalyst for the cycloaddition reaction of CO₂ with various epoxides, it mostly exhibits a poor conversion and requires drastic reaction conditions such as high temperature and pressure for a good conversion. On the other hand, the synergy of the two-dimensional clay, AC with the MIL-101(Cr) yielded novel nanocomposites which act as efficient catalysts under ambient conditions. One of the composites exhibits excellent catalytic efficiency showing 99.9% conversion with a variety of substrates at atmospheric pressure. This composite acts as a heterogeneous catalyst with recycling efficiency and also exhibits highly enhanced solution processability compared to the pristine MOF. It is believed that the present work would open a new route towards the fabrication of MOF-clay composites for promising energy and environmental applications like CO₂ conversion and enhance the scope of novel MOF composites with enhanced functions.

Experimental

Materials

No further purification was done to any of the commercially available reagents or solvents that were used. Terephthalic acid (C₈H₆O₄), chromium nitrate nonahydrate (Cr(NO₃)₃·9H₂O), magnesium chloride hexahydrate (MgCl₂·6H₂O), 3-aminopropyltrimethoxysilane (APTMS), ammonium fluoride (NH₄F), tetrabutylammonium bromide (Bu₄NBr), epichlorohydrin (EPH), styrene oxide (SO), propylene oxide (PO), allyl glycidyl ether (AGE), butyl glycidyl ether (BGE), and epoxy butane (EB) were purchased from Sigma-Aldrich Chemical Company, tetrabutylammonium chloride (TBAC) was purchased from TCI Chemicals (India) Pvt. Ltd. and tetrabutylammonium iodide (TBAI) was purchased from CDH Chemicals.

Table 2 Cycloaddition of CO₂ to different epoxides using MIL-101(Cr)/AC-2 as the heterogeneous catalyst^a

					
Entry	Substrates	Products	Temperature (°C)	Time (h)	Conversion (%)
1			30	6	99.9
2			30	6	99.9
3			40	6	99.9
4			40	12	99.9
5			40	15	99.9
6			40	48	99.9

^a Reaction conditions: 9.2 mmol respective epoxide substrates, 30 mg activated catalyst and 0.92 mmol (296 mg) TBA⁺Br[−] under 1.0 bar CO₂ and at the optimized temperature (30/40 °C). Conversion (%) were calculated from the ¹H NMR spectra by integration of epoxide peaks (a) versus cyclic carbonate peaks (a') (Fig. S20–S24†).

Physical measurements

Powder X-ray diffraction (PXRD) patterns were recorded on a Rigaku Smart Lab SE instrument using Cu-Kα radiation ($\lambda = 1.5406 \text{ \AA}$) in the range of 2–50°. Fourier transform infrared spectroscopy (FTIR), recorded on a Bruker IFS 66v/S spectrophotometer in the area 4000–600 cm^{−1}, was used to characterize the synthesized MOF and its composites. The Mettler Toledo-TGA 850 instrument was used to measure the thermal stability in a N₂ atmosphere within the temperature range 30–800 °C at a heating rate of 5 °C min^{−1}. Morphological studies have been carried out using a Zeiss GeminiSEM 500 Field Emission Electron Microscope (FESEM) by placing samples on a silicon wafer under high vacuum with an accelerating voltage of 20 kV. Energy dispersive spectroscopy (EDS) analysis was performed with an EDAX genesis instrument attached to the FESEM column. Adsorption isotherms of N₂ (at 77 K) were recorded with the desolvated samples using the AUTOSORB iQ2 instrument. To prepare the desolvated samples, **PMIL** and the composites were degassed at 120 °C under 10^{−1} pa vacuum for 12 h before measurements. The surface areas of the samples were calculated from N₂ adsorption data using the ASiQwin software. The temperature-programmed desorption of carbon dioxide (CO₂-TPD) and ammonia (NH₃-TPD) was performed using a BELCAT II instrument. Prior to each measurement *i.e.*, CO₂-TPD and NH₃-TPD, 50 mg of sample were placed in a quartz reactor heated (10 °C

min^{−1}) to 120 °C in a flow of helium (50 ml min^{−1}) for 12 h. After heating the sample was cooled to 30 °C and saturated with CO₂ or NH₃, using a flow of a gas of CO₂ or NH₃ in helium (50 ml min^{−1}) for 30 min. Then, the sample was purged with helium for 30 min to remove the physically absorbed CO₂ or NH₃. Finally, the TPD experiment was carried out with a linear heating rate of 10 °C min^{−1} in a flow of He (50 ml min^{−1}). The desorbed products were analyzed using a mass spectrometer. ¹H NMR spectra were recorded in CDCl₃ solvent using Magritek, Spinsolve Benchtop NMR.

Catalytic study

Prior to catalytic studies, all the catalysts were activated at 120 °C under vacuum for 12 h. The performance of the different catalysts in the CO₂ fixation experiments was checked under different reaction conditions varying the reaction time and temperature and the optimized reaction conditions were used for further catalytic reactions. All the catalytic reactions were performed by taking 30 mg of the respective activated catalyst (as entered in Table 1), 0.92 mmol (296 mg) of the co-catalyst tetrabutylammonium bromide (TBA⁺Br[−]) (10 mol% with respect to substrate), and 9.2 mmol of the substrate in a 30 ml Schlenk tube with CO₂ purged at 1 bar (using CO₂ balloon). For the catalytic reaction using a physical mixture of **PMIL** and AC, 95 mg of **PMIL** and 5 mg of AC (5 weight% w.r.t. total amount) were taken. Catalytic reactions were also per-

formed without any catalyst and only using the co-catalyst TBA^+Br^- , at 30 °C and 40 °C (Table 1). Every cycloaddition reaction was carried out under solvent-free conditions in the Schlenk-tube with magnetic stirring. After the reaction, the solid heterogenous catalyst was removed by centrifugation and the product was purified by separation using ethyl acetate and water. The conversion (%) was calculated based on ^1H NMR analysis by integration of epoxide peaks (a) *versus* cyclic carbonate peaks (a') that are circled in the structures (refer to the ^1H NMR spectra in the ESI†). For the recyclability tests, the recovered catalyst was washed with fresh CHCl_3 thoroughly, air-dried and finally was activated at 120 °C under vacuum for 12 h perform further catalytic reactions under identical conditions.

Synthesis

Pristine MIL-101(Cr) (PMIL). PMIL was synthesized by following a literature reported procedure.⁵⁴ In a typical synthesis, $\text{Cr}(\text{NO}_3)_3 \cdot 9\text{H}_2\text{O}$ (1200 mg, 3 mmol) and terephthalic acid (H_2bdc) (400 mg, 3 mmol) were added to water (15 ml, 265 mmol) and stirred for 10 minutes. The resultant suspension was heated under autogenous pressure for 8 h at 220 °C in a Teflon-lined autoclave and then cooled to room temperature. Following centrifugation, the product was separated as a green powder and washed with EtOH. The sample was further purified under refluxed conditions using ethanol and aqueous NH_4F , respectively, as reported in the literature.⁵⁴ Yield: 45%, relative to Cr(III). The phase purity of the sample was checked by PXRD analysis (Fig. 1).

Aminoclay (AC). Aminoclay was synthesized by following a literature reported method.⁵⁵ Typically, aminopropyl-functionalized magnesium phyllosilicate clay was synthesized by adding dropwise 1 ml (5.85 mmol) 3-aminopropyltrimethoxysilane into an aqueous solution of 0.84 g (3.62 mmol) magnesium chloride in ethanol (25 ml) at 25 °C. The solution was agitated for 24 h and reprecipitated from ethanol before being dried. A colourless product was obtained after drying at 40 °C. The phase purity of AC was analyzed by PXRD (Fig. S1†).

MIL-101(Cr)/AC composites. The syntheses of the composites were performed by dispersing AC in water first and then adding the precursor solution of MIL-101(Cr). **MIL-101(Cr)/AC-1** was synthesized *in situ* by a solvothermal method and 45 mg (2.5 weight% of total amount of reactants) of AC was dispersed in 1 ml of water first and then a 10 ml aqueous solution of $\text{Cr}(\text{NO}_3)_3 \cdot 9\text{H}_2\text{O}$ (1200 mg, 3 mmol) was added to it and stirred for 10 min. Then, terephthalic acid (H_2bdc) (400 mg, 3 mmol) was added to the above mixture and the resulting mixture was stirred for 10 min and transferred to an autoclave coated with Teflon. The resultant suspension was heated under autogenous pressure at 220 °C for 8 h and cooled to room temperature. After centrifugation, the green product was separated and washed with ethanol. The sample was purified further using aqueous NH_4F and hot ethanol solutions.⁵⁴ The material was then dried under vacuum. For preparing the other two composites, similar synthetic processes were

adopted where 90 mg (5 weight%) and 138 mg (7.5 weight%) of AC were taken for the synthesis of **MIL-101(Cr)/AC-2** and **MIL-101(Cr)/AC-3**, respectively.

Conflicts of interest

There are no conflicts to declare.

Acknowledgements

A. C. sincerely acknowledges the Department of Science and Technology (DST), New Delhi, India for an INSPIRE Faculty Fellowship (DST/INSPIRE/04/2020/001603). The authors are grateful to the Central University of Haryana, Mahendergarh for infrastructural support and characterization facilities. Jyoti acknowledges CUH for providing a research fellowship during the initial two years of research and UGC, New Delhi for the current Junior Research Fellowship (NTA Ref. No.: 221610140712). S. K. acknowledges CSIR, New Delhi for Senior Research Fellowship (09/1152(0021)/2020-EMR-I). Jyoti also acknowledges Ms. Ekta and Mr. Aman Kumar for their valuable contribution in analysing some NMR data. The authors gratefully acknowledge Prof. T. K. Maji of JNCASR, Bangalore and Prof. Richard Layfield and Dr Siddhartha De of University of Sussex, UK for some of the measurements.

References

- Carbon dioxide: projected emissions and concentrations, https://ipcc-data.org/observ/ddc_co2.html.
- E. S. S. Pérez, C. R. Murdock, S. A. Didas and C. W. Jones, *Chem. Rev.*, 2016, **116**, 11840.
- A. Kätelhöhn, R. Meys, S. Deutz, S. Suh and A. Bardow, *Proc. Natl. Acad. Sci. U. S. A.*, 2019, **116**, 11187.
- Q. Liu, L. Wu, R. Jackstell and M. Beller, *Nat. Commun.*, 2015, **6**, 5933.
- M. Ding, R. W. Flaig, H.-L. Jiang and O. M. Yaghi, *Chem. Soc. Rev.*, 2019, **48**, 2783.
- C. Martin, G. Fiorani and A. W. Kleij, *ACS Catal.*, 2015, **5**, 1353.
- J. Chun, S. Kang, N. Kang, S. M. Lee, H. J. Kimb and S. U. Son, *J. Mater. Chem. A*, 2013, **1**, 5517.
- L. Guo, R. Dou, Y. Wu, R. Zhang, L. Wang, Y. Wang, Z. Gong, J. Chen and X. Wu, *ACS Sustainable Chem. Eng.*, 2019, **7**, 16585.
- S. Saengsaen, S. D. Gobbo and V. D'Elia, *Chem. Eng. Res. Des.*, 2023, **191**, 630.
- Y. Chen, R. Luo, Q. Xu, J. Jiang, X. Zhou and H. Ji, *ChemSusChem*, 2017, **10**, 2534.
- H.-C. Zhou, J. R. Long and O. M. Yaghi, *Chem. Rev.*, 2012, **112**, 673.
- T. Islamoglu, Z. Chen, M. C. Wasson, C. T. Buru, K. O. Kirlikovali, U. Afrin, M. R. Mian and O. K. Farha, *Chem. Rev.*, 2020, **120**, 8130.

- 13 S. Roy, A. Chakraborty and T. K. Maji, *Coord. Chem. Rev.*, 2014, **273**, 139.
- 14 P. Yadav, P. Bhardwaj, M. Maruthi, A. Chakraborty and P. Kanoo, *Dalton Trans.*, 2023, **52**, 11725.
- 15 P. Yadav, S. Kumari, A. Yadav, P. Bhardwaj, M. Maruthi, A. Chakraborty and P. Kanoo, *ACS Omega*, 2023, **8**, 28367.
- 16 A. Yadav, S. Kumari, P. Yadav, A. Hazra, A. Chakraborty and P. Kanoo, *Dalton Trans.*, 2022, **51**, 15496.
- 17 A. Yadav and P. Kanoo, *Chem. – Asian J.*, 2019, **14**, 3531.
- 18 A. Bavykina, N. Kolobov, I. S. Khan, J. A. Bau, A. Ramirez and J. Gascon, *Chem. Rev.*, 2020, **120**(16), 8468.
- 19 L. Zhu, X.-Q. Liu, H.-L. Jiang and L.-B. Sun, *Chem. Rev.*, 2017, **117**, 8129.
- 20 M. H. Beyzavi, C. J. Stephenson, Y. Liu, O. Karagiari, J. T. Hupp and O. K. Farha, *Front. Energy Res.*, 2015, **2**, 1.
- 21 C. Liu, L. Shi, J. Zhang and J. Sun, *Chem. Eng. J.*, 2022, **427**, 131633.
- 22 Z. Gao, L. Liang, X. Zhang, P. Xu and J. Sun, *ACS Appl. Mater. Interfaces*, 2021, **13**, 61334.
- 23 S. Subramanian, J. Park, J. Byun, Y. Jung and T. C. Yavuz, *ACS Appl. Mater. Interfaces*, 2018, **10**, 9478.
- 24 G. Férey, C. Serre, C. M. Draznieks, F. Millange, S. Surblé, J. Dutour and I. Margiolaki, *Angew. Chem., Int. Ed.*, 2004, **43**, 6296.
- 25 S. Bhattacharjee, C. Chen and W.-S. Ahn, *RSC Adv.*, 2014, **4**, 52500.
- 26 M. Y. Zorainy, M. G. Alalm, S. Kaliaguine and D. C. Boffito, *J. Mater. Chem. A*, 2021, **9**, 22159.
- 27 O. V. Zalomaeva, A. M. Chibiryayev, K. A. Kovalenko, O. A. Kholdeeva, B. S. Balzhinimaev and V. P. Fedin, *J. Catal.*, 2013, **298**, 179.
- 28 O. V. Zalomaeva, N. V. Maksimchuk, A. M. Chibiryayev, K. A. Kovalenko, V. P. Fedin and B. S. Balzhinimaev, *J. Energy Chem.*, 2013, **22**, 130.
- 29 J. Kim, S.-N. Kim, H.-G. Jang, G. Seo and W.-S. Ahn, *Appl. Catal., A*, 2013, **453**, 175.
- 30 E. Akimana, J. Wang, N. V. Likhanova, S. Chaemchuen and F. Verpoort, *Catalysts*, 2020, **10**, 453.
- 31 A. Marandi, M. Bahadori, S. Tangestaninejad, M. Moghadam, V. Mirkhani, I. Mohammadpoor-Baltork, R. Frohnhoven, S. Mathur, A. Sandleben and A. Klein, *New J. Chem.*, 2019, **43**, 15585.
- 32 B. Aguila, Q. Sun, X. Wang, E. O'Rourke, A. M. Al-Enizi, A. Nafady and S. Ma, *Angew. Chem., Int. Ed.*, 2018, **57**, 1.
- 33 M. Ding and H.-L. Jiang, *ACS Catal.*, 2018, **8**, 3194.
- 34 M. Bahadori, S. Tangestaninejad, M. Bertmer, M. Moghadam, V. Mirkhani, I. Mohammadpoor-Baltork, R. Kardanpour and F. Zadehahmadi, *ACS Sustainable Chem. Eng.*, 2019, **7**, 3962.
- 35 F. Li, Y. Chen, A. Gao, W. Tong, C. Ji, Y. Cheng and Y.-H. Zhou, *New J. Chem.*, 2022, **46**, 18418.
- 36 Y. Liu, J. Li, Z. Zhang, Y. Hou, L. Wang and J. Zhang, *Inorg. Chem.*, 2022, **61**, 17438.
- 37 W. Dai, P. Mao, Y. Liu, S. Zhang, B. Li, L. Yang, X. Luo and J. Zou, *J. CO₂ Util.*, 2020, **36**, 295.
- 38 Y. Sun, H. Huang, H. Vardhan, B. Aguila, C. Zhong, J. A. Perman, A. M. Al-Enizi, A. Nafady and S. Ma, *ACS Appl. Mater. Interfaces*, 2018, **10**, 27124.
- 39 D. Liu, G. Li and H. Liu, *Appl. Surf. Sci.*, 2018, **428**, 218.
- 40 L.-F. Xiong, R. Bu, S.-L. Yang and E.-Q. Gao, *Microporous Mesoporous Mater.*, 2022, **339**, 111984.
- 41 L.-J. Zhou, W. Sun, N.-N. Yang, P. Li, T. Gong, W.-J. Sun, Q. Sui and E.-Q. Gao, *ChemSusChem*, 2019, **12**, 2202.
- 42 W.-S. Liu, L.-J. Zhou, G. Li, S.-L. Yang and E.-Q. Gao, *ACS Sustainable Chem. Eng.*, 2021, **9**, 1880.
- 43 L.-F. Xiong, L.-J. Zhou, R. Bu, S.-L. Yang and E.-Q. Gao, *Microporous Mesoporous Mater.*, 2022, **330**, 111601.
- 44 J. Long, W. Dai, M. Zou, B. Li, S. Zhang, L. Yang, J. Mao, P. Mao, S. Luo and X. Luo, *Microporous Mesoporous Mater.*, 2021, **318**, 111027.
- 45 Y. Jiang, D. Li, Y. Zhao and J. Sun, *J. Colloid Interface Sci.*, 2022, **618**, 22.
- 46 D. Ma, B. Li, K. Liu, X. Zhang, W. Zou, Y. Yang, G. Li, Z. Shi and S. Feng, *J. Mater. Chem. A*, 2015, **3**, 23136.
- 47 Y. Jiang, Z. Wang, P. Xu and J. Sun, *Cryst. Growth Des.*, 2021, **21**, 3689.
- 48 Q.-L. Zhu and Q. Xu, *Chem. Soc. Rev.*, 2014, **43**, 5468.
- 49 R. Lin, M. Chai, Y. Zhou, V. Chen, T. D. Bennett and J. Hou, *Chem. Soc. Rev.*, 2023, **52**, 4149.
- 50 K. R. Datta, A. Achari and M. Eswaramoorthy, *J. Mater. Chem. A*, 2013, **1**, 6707.
- 51 A. Chakraborty, S. Laha, K. Kamali, C. Narayana, M. Eswaramoorthy and T. K. Maji, *Inorg. Chem.*, 2017, **56**, 9426.
- 52 A. Chakraborty, A. Achari, M. Eswaramoorthy and T. K. Maji, *Chem. Commun.*, 2016, **52**, 11378.
- 53 A. Chakraborty, S. Roy, M. Eswaramoorthy and T. K. Maji, *J. Mater. Chem. A*, 2017, **5**, 8423.
- 54 D. Jiang, A. D. Burrows and K. J. Edler, *CrystEngComm*, 2011, **13**, 6916.
- 55 G. Johnsy, K. K. R. Datta, V. A. Sajeevkumar, S. N. Sabapathy, A. S. Bawa and M. Eswaramoorthy, *ACS Appl. Mater. Interfaces*, 2009, **1**, 2796.
- 56 X. Quan, Z. Sun, H. Meng, Y. Han, J. Wu, J. Xu, Y. Xu and X. Zhang, *Dalton Trans.*, 2019, **48**, 5384.
- 57 A. Rehman, F. Saleem, F. Javed, A. Ikhlaiq, S. W. Ahmad and A. Harvey, *J. Environ. Chem. Eng.*, 2021, **9**, 105113.
- 58 J.-Q. Wang, D.-L. Kong, J.-Y. Chen, F. Cai and L.-N. He, *J. Mol. Catal. A: Chem.*, 2006, **249**, 143.
- 59 A. K. Gupta, N. Guhab, S. Krishnanb, P. Mathura and D. K. Rai, *J. CO₂ Util.*, 2020, **39**, 101173.
- 60 B. Parmar, P. Patel, R. S. Pillai, R. K. Tak, R. I. Kureshy, N.-u. H. Khan and E. Suresh, *Inorg. Chem.*, 2019, **58**, 10084.
- 61 D. Tanaka, A. Henke, K. Albrecht, M. Moeller, K. Nakagawa, S. Kitagawa and J. Groll, *Nat. Chem.*, 2010, **2**, 410.
- 62 T. Kiyonaga, M. Higuchi, T. Kajiwar, Y. Takashima, J. Duan, K. Nagashima and S. Kitagawa, *Chem. Commun.*, 2015, **51**, 2728.
- 63 R. Das, T. Ezhil, A. S. Palakkal, D. Muthukumar, R. S. Pillai and C. M. Nagaraja, *J. Mater. Chem. A*, 2021, **9**, 23127.